Original Article

Computer-aided Diagnosis of Polyp Classification Using Scale Invariant Features and Extreme Gradient Boosting

S. Don

Department of Computer Science and Applications, Amrita School of Computing, Amrita Vishwa Vidyapeetham, Kollam, Kerala, India

Abstract

Aims: Analysis of colonoscopy images is an important diagnostic procedure in the identification of colorectal cancer. It has been observed that owing to advancements in technology, numerous machine-learning models now excel in the analysis of colorectal polyps classification. This work focused on developing a framework that can classify polyps using images during colonoscopy. **Materials and Methods:** First, the images were corrected by removing their spectral reflection. Second, feature pools were obtained by applying Radon transform (θ=45, 90, 135, and 180). From the Radon transform, fractal dimension was calculated as a feature vector combined with Zernike moment obtained from the Zernike features. Finally, Extreme Gradient Boosting (XGBoost) algorithm was applied for the classification and to compare it with state-of-the-art methods. **Results:** The experimental results obtained with the proposed framework have been reported, cross-validated, and discussed. The proposed method gives a classification accuracy of 93% for light XGBoost and 92% for XGBoost. **Conclusion:** This study shows that by applying scale invariant features over a small dataset, XGBoost outperforms state-of-the-art methods when it comes to polyp classification.

Keywords: Fractal, gradient boosting algorithm, polyps, Radon transform, spectral reflection, Zernike movement

Received on: 06-03-2023 **Review completed on:** 23-06-2023 **Accepted on:** 26-06-2023 **Published on:** 18-09-2023

Introduction

Colonoscopy is an endoscopic procedure done by doctors to examine the large intestine of a person to find colorectal cancer or polyps using a tube with a light and camera. The captured images are influenced by the reflection of light, and this reflection is called specular reflection. Since removing specular reflection is significant for analysis, there needs to be a method to locate the reflected region and restore those regions. Other methods for colon screening are sigmoidoscopy[1] and virtual colonoscopy.[2] Sigmoidoscopy, which can be used only for examining larger part of the intestine, has its own complications, such as bleeding and inflammation of peritonitis. Whereas, virtual colonoscopy is a noninvasive approach that uses computed tomography Nuclear Magnetic Resonance (NMR) scan to find polyps at the early stage and treat them easily. If a lesion is detected, the colonoscopy procedure can remove the lesion. The failure of detecting colon cancer region leads to the patient's life being in a critical stage. Thus, inpainting the specular reflection on the surface of the polyp is important for automated classification of polyp. The type of texture features is selected by the machine-learning algorithm for training purposes. Segmenting the specular highlights in an image is either done by detecting gray scale intensity or color changes. After segmenting the specular highlights, the missing areas are filled. Depending on the application, different solutions exist for specular detection and inpainting.

There are several machine-learning algorithms devoted to the identification of specular reflection and inpainting. Thomas[3] proposed a method for specular reflection removal based on specular deconvolution algorithms. For an image with complex texture, color segmentation still lack to segment correctly. There needs to be an alternative approach. Tan and Ikeuchi.[4] suggest a method to separate specular reflection components based on chromaticity-based-iteration with regard to logarithmic differentiation of the specular free image. Islam *et al*.[5] suggest a multistage approach for determining the specular reflection

Address for correspondence: Dr. S. Don, Department of Computer Science and Applications, Amrita School of Computing, Amrita Vishwa Vidyapeetham, Amritapuri, Kollam, Kerala, India.
E-mail: dons@am.amrita.edu

Access this article online

Quick Response Code:

Website: www.jmp.org.in

DOI: 10.4103/jmp.jmp_29_23

How to cite this article: Don S. Computer-aided diagnosis of polyp classification using scale invariant features and extreme gradient boosting. J Med Phys 2023;48:230-7.

detection and inpainting. The results are promising and can be used in multiple fields. A detailed analysis of specular reflection detection has been reported by Jayasinghe *et al*.[6] Several researchers[7-9] have introduced more complex models for removing reflection components from the collected specular reflection and inpainting. It has been observed that retrieval of specular reflectance from the initial stage of image analysis is important in many medical applications. This reflection from the image plane influences the quality of decision-making, particularly in the domain of image classification. Identifying the specular reflectance region and reconstructing the missing region in an important problem is the computer's vision. Image inpainting[10] is a process of reconstructing the missing or corrupted region in an image. This method can be broadly classified into two: diffusion-based approaches and exemplar-based approach. In this work, exemplar-based image inpainting approach proposed by Criminisi[11] was chosen. The computational efficiency of this method was achieved by a block-based sampling process.

Figure 1 shows the proposed architecture for polyp classification. First, the image inpainting is done on the polyp images. The second step is to extract suitable features for the classification. In this work, rotation invariant texture features were considered using Radon transform, fractal dimension (FD), and Zernike movement. Radon transform,[12] which is both a translation and rotation invariant, preserves variations in pixel intensities. In the Radon transform, a small number of directions is sufficient to characterize the properties of radon. In the study, the proposed feature selection method is first calculating the Radon transform angle as θ 45:90:135:180 from the output of the preprocessed image. Secondly, the output of the Radon transform is given as an input to FD and Zernike moments. FD refers to the dimension used for understanding the fractal characteristic present in a given image.[13] Here, FD was applied to the output of Radon transfer to obtain a single feature vector. The method applied to measure FD was Higuchi's FD.[14] The last method considered for feature extraction was the Zernike polynomials. Zernike moments type features are rotation invariant that map an image into a set of complex Zernike polynomial, which represents the properties of the images with no overlap of information between various moments. By combining the feature vectors of Zernike moments and FD, 13 feature attributes of each image were obtained, and this feature set was passed to the classification module. For the classification, Extreme Gradient Boosting (XGBoost) was used, and it was compared with Light Gradient Boosting and the Random Forest algorithm. Classifying images using very few sample datasets has been actively researched in recent years. A systematic and extensive overview of classification with small datasets was reported in.[15-17] The remainder of this paper has been organized as follows: Section 2 discusses the methods considered for feature extraction and classification. Section 3 presents the experimental results and finally concludes with the future scope.

Materials and Methods

Datasets selection

In this study, images from CVC-Clinic DB[18] and KVasir[19] datasets were used. CVC-Clinic DB contains 31 short colonoscopy videos with a total of 612 images taken from 23 patients. This database contains several examples of polyps and ground truth mask corresponding to the region covered by polyp with a resolution of 384 × 288. Kvasir-SEG DB contains 1000 polyp images under various class labels for classification purposes. The resolution of the Kvasir-SEG varies from 332 × 487–1920 × 1072. A total of 605 smaller sets of images were considered for the experiment; out of that, 550 images are from CVC-Clinic, and 55 images are from KVasir dataset. For the experiment, the cropped image was normalized with a resolution of 300 × 300. The proposed method consists of three stages: preprocessing, feature extraction, and classification. Preprocessing aimed at performing image normalization and inpainting those images that contained specular reflection. The second stage was the feature extraction part which extracted features from the polyp images. These features were then used in the training and classification stage.

Specular reflection removal

Specular reflection refers to bright patches of pixels within the image during colonoscopy. Identifying such patches and their removal could enhance the performance of the classification and simplify the diagnostic procedure. Locating the bright patches in the images is challenging due to various illuminations. In this paper, a threshold based approach was adopted to locate the region, followed by a morphological operation. Figure 2 shows a random image that contains a specular region, its mask region, and the result obtained after inpainting.

Once the region of interest was identified, the next step was to remove the specular reflection. A common approach in image inpainting is that the bright patches of pixels can be filled with similar texture in the surrounding region.[20] The method that was followed in this paper for filling the target region is a patch-by-patch operation based on exemplar. The selection of

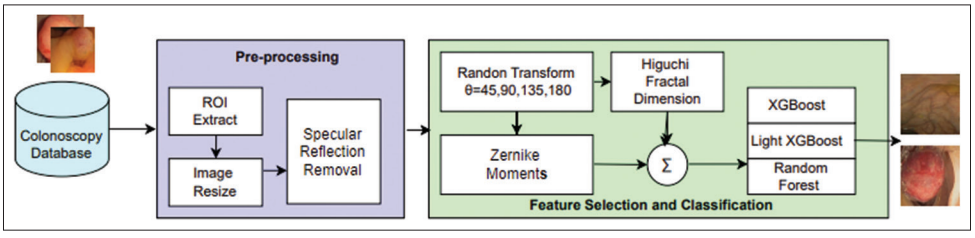

Figure 1: Proposed framework for polyp classification

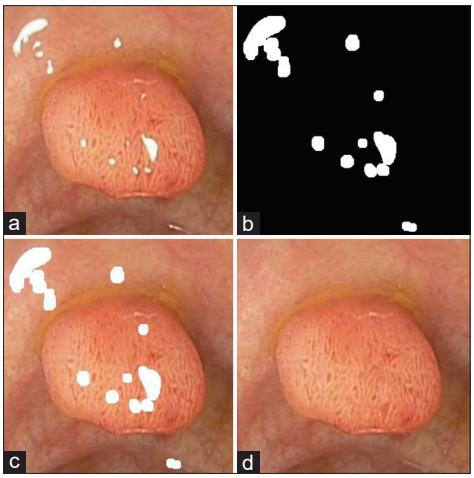

Figure 2: (a) Original image, (b) mask of the specular region, (c) superimposing the mask over the image, (d) inpainted image

a patch that is a good candidate for inpainting was done based on isophote-driven image sampling and the available known information about the patch. Figure 3 shows the structure propagation by exemplar-based texture analysis.

Given the patch ψ_p, source ϕ and target region Ω and $\delta\Omega$ be its contour. We want to synthesize the area delimited by Ψ_p, such that $p \in \delta\Omega$. The iterative algorithm works as follows: given the input image and every pixel has a confidence value C (p). First, we identify the boundaries. If there is a change in the previous iteration, the boundary region needs to be recalculated. Once this is done, the next step is to compute P (p), i.e. the priority of every pixel on this boundary.

P (p) = C (p). D (p)……(1)

where C (p) is the confidence term and D (p) is the data term, defines as

$$C(p) = \frac{\sum_{q \in \Psi_p \cap \Omega} C(q)}{|\Psi_p|} \quad \text{and} \quad D(p) = \left| \frac{\nabla I_P^{\perp} . n_P}{\alpha} \right|$$

At the initial state C(p) = 0 $\forall p \in \Omega$ and C(P) =1 $\forall p \in I - \Omega$. Once the patch has done, next is to find the patch with highest priority ψ_p and fill the data extracted $\hat{p} = \text{argmax}_{p \in \delta\Omega'} P(p)$ from the source region ϕ. So the best exemplar $\hat{\Psi}(q) = \text{argmind}(\Psi_p, \Psi_q)$, where $d(\Psi_p, \Psi_q)$ is the distance between two patches. Once the best exemplar is identified, the value of each pixel to be filled, $p' \mid p' \in \Psi_{\hat{p} \cap \Omega}$ is copied from $\hat{\Psi}(q)$. Finally update the confidence value with the highest value.

Radon transform

Radon transform is a tool that is used in various applications such as medical imaging, radar imaging, and remote sensing applications. It is a projection of the gray level intensity value

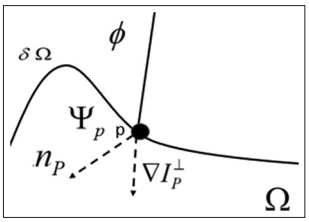

Figure 3: Exemplar based texture analysis

along a radial line at a specific angle (ρ, θ)

$\rho_0 = x\cos\theta_0 + y\sin\theta_0$ ----------(2)

Which can be represented as

$$\text{RT}(\rho_0, \theta_0) = \iint I(x,y)\delta(x\cos\theta_0 + y\sin\theta_0 - \rho_0) \text{ ----------(3)}$$

When (x_0, y_0) are fixed, then the sum over the sinusoid of equation $\rho_0 = x_0 Cos\theta_0 + y_0 Sin\theta_0$ in the random space will yield the intensity of the pixel at coordinate (x_0, y_0) in the image plane. In our approach, θ is considered at interval of 45° with $\theta_{\min} = 0$ and $\theta_{\max} = 180^0$.

Higuchi fractal dimension

FD refers to the dimension used for fractal characteristics and can be used for signal and image processing. In our approach, Higuchi FD method was applied to estimate the FD. This method is suitable for 1D discrete time series. The algorithm was computed as follows: the sample inputs are the values obtained from RT. Since θ varies from (0:45:180), there were 5 discrete samples with a size of 273 each. The FD for each sample was calculated in the following ways.

For a given time series $x(1), x(2), .., E(N)$, the algorithm constructs k new time series for m = 1, 2,….k $X_m^k = x[m], x[m+k], ..., x[m + int((N - m)/k) * k)$,

where k and m are integers. The length of X_m^k is defined as $L_m^k = \left[\frac{1}{k} \sum_{i=1}^{(N-m)/k} |x[m+ik] - x[m+(i-1)k]| . \left\langle \frac{N-1}{\text{int}((N-m)/k) * k} \right\rangle \right]$, where N is the total number of samples and $\frac{N-1}{(\text{int}(N-m)/k) * k)}$, the normalized factor. For the time interval k, L (k) is calculated as the mean of K values L_K for $m = 1, 2, 3, ...k$. The data should fall on a straight line with a slope equal to FD. Therefore, HFD is the slope of the line that fits the pair $\ln[L_k], \ln[1/k]$.

Zernike moment

This Zernike movement is the mapping of an image into Zernike polynomials

$$Z_{n,m} = \frac{n+1}{\lambda N} \sum_{c=0}^{N-1} \sum_{r=0}^{N-1} f(c,r) V^*_{n,m}(c,r) \text{ ……(4)}$$

where $n, m \in N_0$ and N_0 be nonnegative integers. For an image with size of N × N for $0 \le \rho_\sigma \le 1$ and $0 \le \theta_{cr} \le 2\pi$.

$cr \in N_0^2$, $f(c,r)$ is the image function, v is the complex Zernike basis function and λ_N is the unit circle. Equ (4) can be rewritten as $Z_{n,m} = \frac{n+1}{\lambda N}\sum_{c=0}^{N-1}\sum_{r=0}^{N-1} f(c,r)R_{n,m}(\rho\sigma)e^{-jm\theta_{cr}}$ and $R_{n,m(.)}$ is called radial polynomial and defined as

$$R_{n,m} = \sum_{s=0}^{(n-|m|)/2} (-1)^s \frac{(n-s)!}{s!\left(\frac{n+|m|}{2}-s\right)!\left(\frac{n-|m|}{2}-s\right)!}\rho^{n-2s}$$ where

and ρσ are θ_{cr} the transformed distance and phase at pixel (c, r).

$$\rho_{cr} = \frac{\sqrt{(2c-N+1)^2+(2r-N+1)^2}}{N} \quad \text{.....(5)}$$

and $\theta_{cr} = \tan^{-1}\left(\frac{N-1-2r}{2c-N+1}\right)$ .....(6)

Thus, the Zernike moments obtained from the above equation is a complex quantity. $|Z_{nm}| = \sqrt{R_{zm}^2 + I_{zm}^2}$, zm denotes the shape information or the feature obtained for specific Zernike moment (n) and the repetition factor (m). We can go for higher order moment for better accuracy.[21]

Classification model

Supervised learning methods have been used widely as a classifier in medical diagnosis of endoscopic images. Amayeh *et al*[22] utilizes support vector machine for automated colorectal polyp classification based on a clinical prediction model. Surya Prasath[23] suggest a polyp recognition in capsule endoscopy using colon features based on chromaticity histogram integrated with Zernike movement. In the image classification task, the type of feature extraction directly affects the performance. Hence, selection of an efficient classifier becomes important in many applications. The XGBoost algorithm was applied to the feature set to predict the binary outcome (polyp/nonpolyp [NP]). The performance of the classifier was compared with Light Gradient Boosting Machine and Random Forest. From the literature survey, it was observed that XGBoost classifier can be used as a platform to predict the polyp images because it works well based on the relatively small dataset. It also does not require any assumption, regardless of the data distribution.[24] Suppose a given dataset contains n samples and k features, then we can represent it as $D = \{(x_i, y_i) \mid x_i \cup R^m, y_i \in R\}$. The algorithm builds k subtrees satisfied by the expression

$$\hat{y}^{(t)} = \sum_{k=1}^{t} f_k(x_i), f_k \in F \quad \text{.....(7)}$$

$$= \hat{y}_i^{(t-1)} + f_t(x_i)$$, where $\hat{y}_i^{(t-1)}$ is the sum of the predicted value of the previous iteration. F is a set of decision tree, i.e., $F = \{f(x) = w_q(x)\}, (Q: R^m \to T, w \in R^T)$, $w_q(x)$ is the weight of the leaf nodes. The main goal of XG Boost is to learn "k" subtrees and minimize the following regularized objectives

$$L(\phi) = \sum_{i=1}^{n} l(\hat{yi}, yi) + \sum_{k=1}^{K} \Omega f(k), \quad \text{.....(8)}$$

Where $\Omega f(k) = \gamma T + \frac{1}{2}\lambda\|w\|^2$ here l is a loss function between the estimated value $\hat{yi}$ and the true value *yi*.

$\hat{yi}^{(t)} = \hat{yi}^{(t-1)} + fk(xi)$ which is sum of predicted value of the previous iteration. Thus $L(\theta) = \sum_{i=1}^{n} l(\hat{yi}^{(t-1)} + f_t(xi), yi) + \Omega(f_k)$ since XGBoost carries out Taylor series of the objective function, removing the higher order leads to the objective function.

$$L^{(t)} = \sum_{i=1}^{n}\left[l(y_i, \hat{y}_i^{(t-1)}) + g_i f_t(x_i) + \frac{1}{2}h_i f_t^2(x_i)\right] + \Omega(f_k)$$ where g_i and *hi* are the first and second derivatives of loss function. Since the residual between prediction score $\hat{y}_i^{(t-1)}$ and *yi* does not affect optimization so modified as:

$$L^{(t)} = \sum_{i=1}^{n}\left[g_i f_t(x_i) + \frac{1}{2}h_i f_t^2(x_i)\right] + \Omega(f_k) \quad \text{.....(9)}$$

the iterative process of the tree model finally transformed to iteration of the leaf node and the optimal score is $w_j^* = -\frac{G_j}{H_j + \lambda}$ where $G_j = \sum_{i=1}^{I_j} g_j$ and $H_j = \sum_{i=1}^{I_j} h_j$ substituting this we obtained the final objective function $O_j = -\frac{1}{2}\sum_{j=1}^{T}\frac{G_j^2}{H_j+\lambda} + \gamma T$ a fine tune of hyper-parameter is needed that require additional time to get the final solution.

Results

The image set for the experiment consists of 605 images, out of which 227 images belong to polyps (P) and 378 images belong to NP; the set was used to build both the training set and testing set. A total of 363 samples from both categories (N/NP) were considered for the training set, with the test size having a varying sample set of 20%, 30%, 40%, and 50%, respectively. A framework was developed with a smaller dataset for classification to demonstrate that the framework can achieve improved performance compared to a traditional tree-based classifier.

The performance of the proposed framework was evaluated in terms of Precision, Recall, and F-measures. Finally, there was a comparison made with others' work in terms of accuracy, sensitivity/recall and specificity. Features were generated from the colonoscopy images. First, the input image was normalized, inpainted, and the preprocessed image was sent to the feature extraction module. Figure 4 shows the results of a random set of images after the preprocessing stages. The output of the preprocessing stage was first processed by the Radon transform, and the output of the Radon transform is a single vector feature value that was given to the FD module. Here, the technique considered was Higuchi FD. The output of the FD was combined with various higher order Zernike moments obtained from Zernike module to form a feature set of size (605 × 13). This feature set was passed to the classifier

module. The aim was to obtain an efficient classification result that could correctly classify both polyp and NP images and evaluate them in terms of Precision, Recall, and F-measure. It was observed that by varying the testing samples with a ratio of 20%, 30%, 40%, and 50%, there was an improvement in the evaluation matrix when both XGBoost and Light XGBoost classifiers were applied with a reduced sample set. But in the case of Random Forest, the Precision, Recall and F-measure score was lower than or almost same in few polyp test cases. This shows the performance improvement of gradient boost algorithm compared to traditional tree-based approach. This is because, in gradient boosting, the goal is to train multiple trees one stage at a time to correct the error of the previous fitted one, which, thus, improves the performance. LightGBM[25,26] can accelerate the training process by several times when compared to XGBoost, but both achieve almost

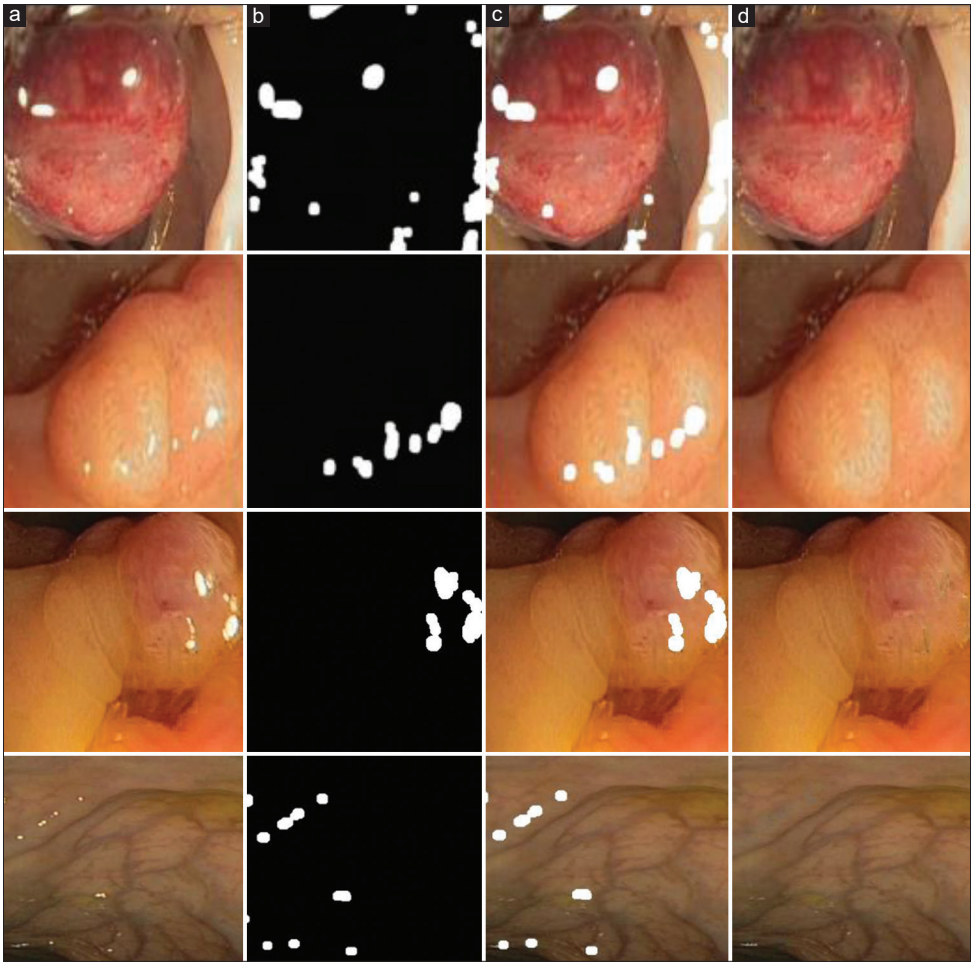

Figure 4: (a) Original image, (b) masked image, (c) overlap image, (d) inpainted image

Table 1: Performance measure of extreme gradient boosting and light extreme gradient boosting

Test size	Task (binary classification)	Method					
		XGBoost			Light XGBoost		
		Precision	Recall	*F*-measure	Precision	Recall	*F*-measure
20	Polyp	0.93	0.87	0.90	0.95	0.85	0.90
	NP	0.92	0.96	0.94	0.91	0.97	0.94
30	Polyp	0.92	0.84	0.88	0.94	0.82	0.88
	NP	0.90	0.95	0.93	0.89	0.96	0.93
40	Polyp	0.88	0.87	0.88	0.87	0.85	0.86
	NP	0.92	0.93	0.93	0.91	0.92	0.92
50	Polyp	0.90	0.90	0.90	0.90	0.88	0.89
	NP	0.94	0.94	0.94	0.93	0.94	0.93

NP: Nonpolyp, XGBoost: Extreme gradient boosting

the same accuracy. It is evident from Tables 1 and 2 that even if the test samples are reduced, a significant test result can be achieved when compared to Random Forest.[27] Table 2 reveals the F-measure score for varying tree sizes (100, 80, 60, and 40). In all cases, the algorithm generated a classification accuracy of 0.57 ± 92.3 (standard deviation ± mean) in all three classifiers. This demonstrates that the proposed framework is a stable one for the purpose of polyp classification.

Figure 5 shows the overall performance of the three methods in terms of accuracy and specificity. The X-axis represents the sample ratio of the dataset during the classification phase. It was observed that in the case of Light XGBoost, the maximum score obtained for accuracy was 93% and for specificity, it was 95% when the test size was 20. Similarly, in the case of XGBoost, the maximum score achieved for accuracy and specificity was 92% and 93%, respectively, when the test

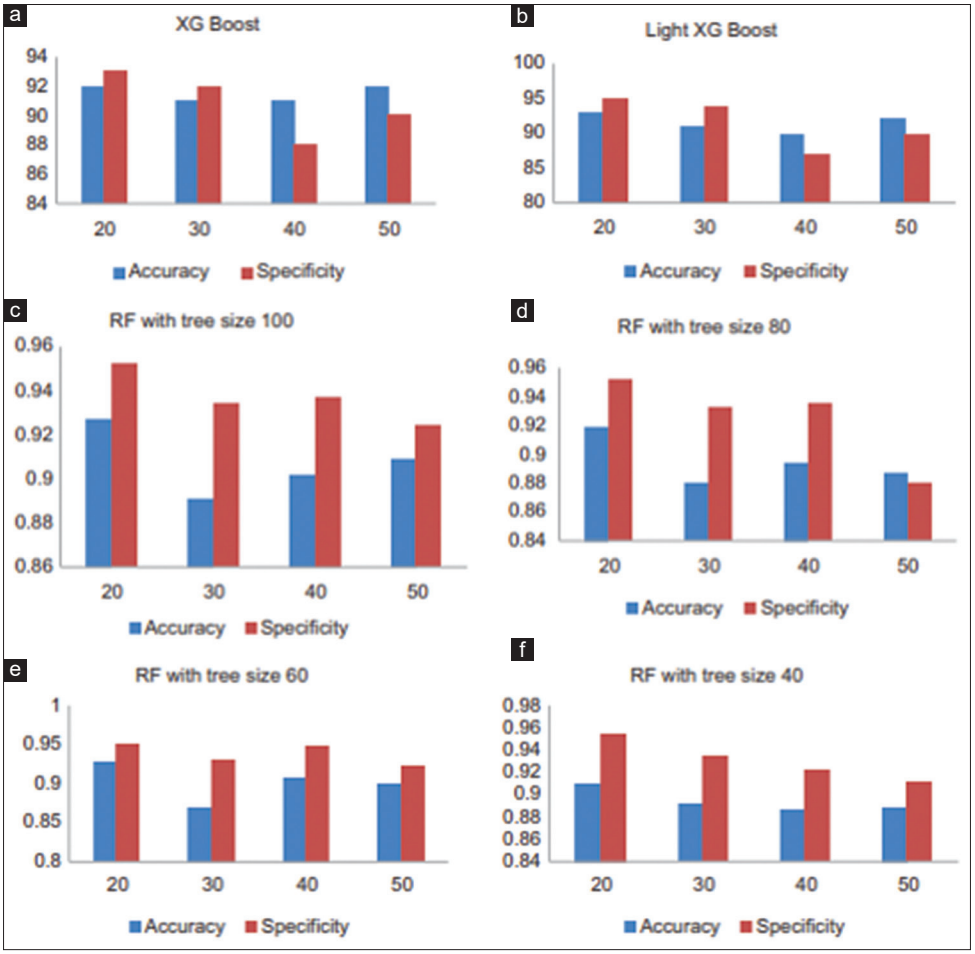

Figure 5: Overall performance of various models in terms of accuracy and specificity. XGBoost: Extreme gradient boosting, RF: Random forest

Table 2: Performance measure for random forest

Test size	Class	RF											
		Tree size=100			Tree size=80			Tree size=60			Tree size=40		
		Precision	Recall	*F*-measure	Precision	Recall	*F*-measure	Precision	Recall	*F*-measure	Precision	Recall	*F*-measure
20	Polyp	0.95	0.85	0.90	0.95	0.83	0.89	0.95	0.85	0.90	0.95	0.89	0.92
	NP	0.91	0.97	0.94	0.90	0.97	0.94	0.91	0.97	0.94	0.93	0.97	0.95
30	Polyp	0.93	0.78	0.85	0.86	0.96	0.91	0.93	0.73	0.82	0.93	0.78	0.85
	NP	0.87	0.96	0.91	0.86	0.96	0.91	0.84	0.96	0.90	0.87	0.96	0.91
40	Polyp	0.94	0.80	0.86	0.94	0.77	0.85	0.95	0.80	0.87	0.92	0.76	0.84
	NP	0.89	0.97	0.92	0.88	0.97	0.92	0.89	0.97	0.93	0.87	0.96	0.91
50	Polyp	0.92	0.83	0.87	0.88	0.81	0.84	0.92	0.80	0.86	0.91	0.79	0.84
	NP	0.90	0.96	0.93	0.89	0.93	0.91	0.89	0.96	0.92	0.88	0.95	0.91

NP: Nonpolyp, XGBoost: Extreme gradient boosting, RF: Random forest

Table 3: Comparison of polyp classification against our proposed model

Study reference	Setup	Models	Accuracy	Sensitivity	Specificity
Grinsven *et al*.[23]	Color, shape and texture	SVM	0.87	0.90	0.80
	Color, shape and texture	SVM optimized	0.91	0.97	0.80
	Color, shape and texture	RF	0.93	0.97	0.87
	Color, shape and texture	Wasp	0.89	0.93	0.80
Patino-Barrientos *et al*.[28]	Kudo's classification schema	SVM	0.83	0.86	-
Gross *et al*.[29]	Statistical features	PS + HT + SA	0.96	0.97	0.94
Li *et al*.[30]	Color and shape features	MLP	0.94	0.93	0.95
Pablo *et al*.[31]	2D texture + 3D features	SVM	0.82	0.72	0.85
Proposed	FD, Zernike movement, Randon transform	XGBoost	0.92	0.93	0.93
	FD, Zernike movement, Randon transform	Light XGBoost	0.93	0.91	0.95
	FD, Zernike movement, Randon transform	RF	0.92	0.90	0.95

2D: Two-dimensional, 3D: Three-dimensional, FD: Fractal dimension, SVM: Support vector machine, XGBoost: Extreme gradient boosting, RF: Random forest, PS: Phase symmetry, HT: Hysteresis thresholding, SA: Simulated annealing, MLP: Multi-layer perceptron

size was 20 and 50. Similarly, for Random Forest, by varying tree sizes, it was observed that with a tree size of 100, the accuracy was 92%, whereas specificity achieved was 95%. When the tree size was changed with various sizes (100, 80, and 40), there was a change in variation in the accuracy during the classification. It has been observed that the type of feature selection with the proposed framework using gradient boosting technique is promising and can be considered a suitable candidate for polyp classification. Table 3 shows a comparison with the current state of the art in terms of accuracy, sensitivity, and specificity for our proposed model. The values of the proposed methods are the ones from the testing set during the experiment. It has been observed that this approach offers more flexibility with the reduced dataset for polyp classification.

Conclusion

This work proposed a framework for computer-aided diagnosis of polyp classification based on scale-invariant feature sets with small datasets using three different classifiers. The features considered for the study show that the performance of the classifier was computationally efficient in terms of Precision, Recall, and F-measure. The test case was conducted with varying sizes, and it was observed that XGBoost and Light XGBoost achieved an accuracy of 92% and specificity of 93% for polyps. The results are promising, and the framework can be useful for the analysis of colonoscopy images.

Financial support and sponsorship

Nil.

Conflicts of interest

There are no conflicts of interest.

References

1. Schoen RE, Pinsky PF, Weissfeld JL, Yokochi LA, Church T, Laiyemo AO, *et al.* Colorectal-cancer incidence and mortality with screening flexible sigmoidoscopy. N Engl J Med 2012;366:2345-57.
2. Dachman AH, Sethi I, Lefere P. Virtual colonoscopy. In: Textbook of Clinical Gastroenterology and Hepatology. 2nd ed. Wiley-Blackwell: UK; 2012. p. 1027-34.
3. Thomas S. Removal of specular reflections in endoscopic images. Acta Polytech J Adv Eng 2006;4632-6.
4. Tan RT, Ikeuchi K. Separating reflection components of textured surfaces using a single image. IEEE Trans Pattern Anal Mach Intell 2005;27:178-93.
5. Islam MN, Tahtali M, Pickering M. Specular reflection detection and inpainting in transparent object through MSPLFI. Remote Sens 2021;13:455.
6. Jayasinghe D, Abeysinghe C, Opanayaka R, Dinalankara R, Silva BN, Wijesinghe RE, *et al*. Minimizing the effect of specular reflection on object detection and pose estimation of bin picking systems using deep learning. Machines 2023;11:91.
7. Shen DF, Guo JJ, Lin GS, Lin JY. Content-aware specular reflection suppression based on adaptive image inpainting and neural network for endoscopic images. Comput Methods Programs Biomed 2020;192:105414.
8. Asif M, Song H, Chen L, Yang J, Frangi AF. Intrinsic layer based automatic specular reflection detection in endoscopic images. Comput Biol Med 2021;128:104106.
9. Kudva V, Prasad K, Guruvare S. Detection of specular reflection and segmentation of cervix region in uterine cervix images for cervical cancer screening. IRBM 2017;38:281-91.
10. Bertalmio M, Sapiro G, Caselles V, Ballester C. Image inpainting. SIGGRAPH 2000; In Proceedings of the 27th annual conference on Computer graphics and interactive techniques:417-24.
11. Criminisi A, Perez P, Toyama K. Object Removal by Exemplar-Based Inpainting. In: IEEE Computer Society Conference on Computer Vision and Pattern Recognition, Proceedings. Madison, WI, USA; 2003.
12. Barrett HH. The radon transform and its applications. Prog Opt 1984;21: 21786.
13. Mandelbrot BB. The Fractal Geometry of Nature. New York: WH Freeman; 1982.
14. Don S, Chung D, Min D, Choi E. Analysis of electrocardiogram signals of arrhythmia and ischemia using fractal and statistical features. J Mech Med Biol 2013;13:1350008.
15. Brigato L, Barz B, Iocchi L, Denzler J. Image classification with small datasets: Overview and benchmark. IEEE Access 2022;10;49233-50.
16. Bornschein J, Visin F, Osindero S. Small data, big decisions: Model selection in the small-data regime. Int Conf Mach Learn 2020;1035-44.
17. Shaikhina T, Khovanova NA. Handling limited datasets with neural networks in medical applications: A small-data approach. Artif Intell Med 2017;75:51-63.
18. Bernal J, Sánchez FJ, Fernández-Esparrach G, Gil D, Rodríguez C, Vilariño F. WM-DOVA maps for accurate polyp highlighting in colonoscopy: Validation versus. Saliency maps from physicians. Comput Med Imaging Graph 2015;43:99-111.
19. Criminisi A, Pérez P, Toyama K. Region filling and object removal

by exemplar-based image inpainting. IEEE Trans Image Process 2004;13:1200-12.
20. Jha D, Smedsrud PH, Riegler MA, Halvorsen P, de Lange T, Johansen D, *et al*. Kvasir-SEG: A segmented polyp dataset. In: Conf. Multimedia Model. 11962: Springer 2020.
21. Akbari M, Mohrekesh M, Najariani K, Karimi N, Samavi S, Soroushmehr SM. Adaptive Specular Reflection Detection and Inpainting in Colonoscopy Video Frames. In: 25th IEEE International Conference on Image Processing (ICIP). Athens, Greece; 2018. p. 3134-8.
22. Amayeh G, Erol A, Bebis G, Nicolescu M. Accurate and efficient computation of high order Zernike moments. In: Bebis G, Boyle R, Koracin D, Parvin B, editors. Advances in Visual Computing. Vol. 3804: LNCS, ISVC; 2005. p. 462-9.
23. M.C.A van Grinsven MC, Scheeve T, Schreuder RM, der Sommen FV, Schoon EJ, de With PH. Image Features for Automated Colorectal Polyp Classification Based on Clinical Prediction Models. Taiwan: IEEE International Conference on Image Processing (ICIP); 2019. p. 210-4.
24. Surya Prasath VB. Polyp detection and segmentation from video capsule endoscopy: A review. J Imaging 2016;3:1.
25. Chen T, Guestrin C. XGBoost: A scalable tree boosting system. KDD 2016;16:13-7.
26. Ke G, Meng Q, Finley T, Wang T, Chen W, Ma W, *et al*. LightGBM: Ahighly efficient gradient boosting decision tree. In: Advances in Neural Information Processing Systems 30 (NIPS 2017). NeurLPS: USA; 2017. p. 3149-57.
27. Zhang H, Si S, Cho-Jui H. GPU Acceleration for large-scale tree boosting. SysML Conf 2018.
28. Patino-Barrientos S, Sierra-Sosa D, Garcia-Zapirain B, Castillo-Olea C, Elmaghraby A. Kudo's classification for colon polyps assessment using a deep learning approach. Appl Sci 2020;10:501.
29. Gross S, Palm S, Tischendorf JJ, Behrens A, Trautwein C, Aach T, Automated classification of colon polyps in endoscopic image data. In: Proceedings SPIE 8315, Medical Imaging 2012: Computer-Aided Diagnosis, 83150W; 2012.
30. Li B, Fan Y, Meng MQ, Qi L. Intestinal Polyp Recognition in Capsule Endoscopy Images Using Color and Shape Features. In: 2009 IEEE International Conference on Robotics and Biomimetics (ROBIO); 2009. p. 1490-4.
31. Mesejo P, Pizarro D, Abergel A, Rouquette O, Beorchia S, Poincloux L, *et al.* Computer-aided classification of gastrointestinal lesions in regular colonoscopy. IEEE Trans Med Imaging 2016;35:2051-63.